

WELDED JOINTS

UDC 620.17:621.791.052:669.715

COMPARATIVE ANALYSIS OF NON-UNIFORMITY OF MECHANICAL PROPERTIES OF WELDED JOINTS OF Al – Mg – Si ALLOYS DURING FRICTION STIR WELDING AND LASER WELDING

S. Yu. Ivanov,¹ O. V. Panchenko,² and V. G. Mikhailov³Translated from *Metallovedenie i Termicheskaya Obrabotka Metallov*, No. 6, pp. 53 – 58, June, 2018.

The properties of the welded joints of 6082-T6 alloy produced by friction stir welding (FSW) and laser welding (LW) were studied. The maximum temperature and microhardness fields in the friction stir-welded joints were shown to be asymmetrical. The concentrated energy input during laser welding yields a narrow heat-affected zone (HAZ) with sharp changes in mechanical properties. The strength of the FSW joint constitutes 72% and that of the LW joint — 67% of the base metal strength. In case of LW, the minimum hardness of the joint corresponds to the metal of the welded joint, while in case of FSW, it corresponds to the heat-affected zone. At the same maximum heating temperature, the hardness of the heat-affected zone of the friction stir-welded joint is lower compared to laser welding due to substantially lower rates of heating and cooling.

Key words: friction stir welding, laser welding, Al – Mg – Si alloy, temperature field, welded joint, microstructure, mechanical properties, non-uniformity.

INTRODUCTION

Poor weldability of aluminum alloys using arc-welding methods prevents them from being widely used for creation of integrated structures. The main problems are: pores formation [1, 2], softening in the heat-affected zone (HAZ) [3, 4], and formation of hot cracks [5 – 7]. The presence of the refractory oxide film on the surface of aluminum does not allow obtaining slot-welded joints by means of arc-welding. High-quality aluminum alloy joints with high strength characteristics can be obtained by using advanced material-joining technologies, such as laser welding (LW) and friction stir welding (FSW). High concentration of energy achieved in a laser beam allows producing joints with narrow HAZ, which is especially important when welding heat-treatable aluminum alloys. The main disadvantages of LW include low beam-power efficiency, pore formation, and evaporation of alloying elements [8, 9].

The friction stir welding is free of the defects associated with metal melting, since the joining of the materials occurs in the solid state (Fig. 1). The application of this technology is significantly restricted by low technological effectiveness, need for expensive equipment and narrow range of the types of welded joints [10].

The mechanisms of welded joint formation by using LW and FSW to join Al – Mg – Si alloys are described in the li-

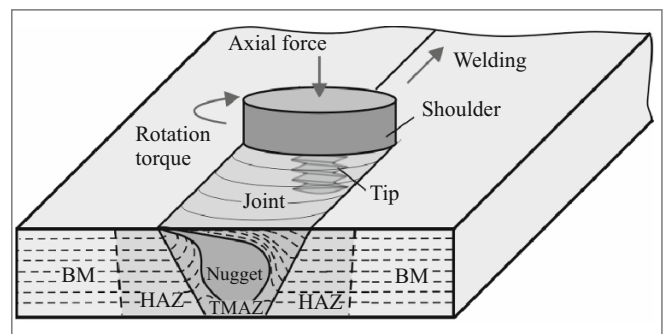


Fig. 1. Schematic illustration of friction stir welding and welded joint (TMAZ — Thermo-mechanically affected zone).

¹ Peter the Great St. Petersburg Polytechnic University (SPPU), St. Petersburg, Russia (e-mail: sergei.yu.ivanov@gmail.com).

² Science and Technology Center “Novel Manufacturing Technologies,” SPPU, St. Petersburg, Russia.

³ Brandenburg University of Technology, Cottbus, Germany.

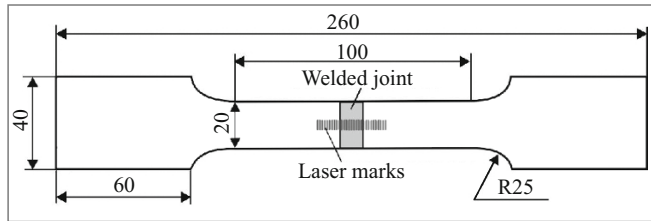


Fig. 2. Schematic of tensile test sample.

temperature in sufficient detail. The majority of publications are focused on establishing the causes of defects and mechanisms of joint formation. However, little information is available describing the effect of the thermal deformation cycle of the welding on distribution of local mechanical properties [11–14].

The objective of this work is to study the effect of the thermal deformation cycles during friction stir welding and laser welding on the formation of local mechanical properties and functionality of the welded joints of Al–Mg–Si alloys.

METHODS OF STUDY

Welded joints of the 4 mm thick plates of aluminum alloy 6082-T6⁴ (Russian analog — AD35-T1) were obtained by using friction stir welding and laser welding. Chemical composition of the alloy is as follows: 0.7% Mg; 1.00% Si; 0.07% Cu; 0.51% Mn; 0.08% Zn; 0.39% Fe. By combining quenching without polymorphic transformation and artificial aging, the yield strength of $\sigma_{0.2} = 298$ MPa, tensile strength of $\sigma_t = 340$ MPa, and percentage of elongation of 22% were achieved. In addition, mechanical properties of the base metal previously subjected to quenching without polymorphic transformation followed by natural aging (T4 condition) were determined.⁵

⁴ T6 — Russian designation T1 (quenching with subsequent aging yielding maximum strength).

⁵ Russian designation — T.

Laser welding was carried out by utilizing a robotic complex Reis RLP 16-TF with fiber laser having a capacity of 15 kW. The plates were welded without grooving and without the use of a filler wire according to the following regimen: welding rate — 50 mm/sec, beam power — 6.3 kW. Friction stir welding was conducted by using a three-axial milling machine UNITECH with a 6.5 mm diameter conic tip with a spirally threaded surface and an 18 mm diameter shoulder. The FSW process parameters were as follows: welding rate — 4.2 mm/sec, rotation speed of the tool — 1120 rpm, and tool axis tilt angle — 2°. In the process of welding, the plates were pushed against a steel substrate with massive clamps, which provided an almost ideal thermal contact between them.

Thermal cycles were measured during the welding process by using the HBM QuantumX MX 609 installation while using Chromel/Alumel thermocouples measuring 0.2 mm in diameter with a frequency of 5 Hz during FSW and 50 Hz during LW. The thermocouples were positioned at various distances from the axis of the joint.

The microstructure was studied by Leica DMI5000M optical microscope with $\times 1000$ magnification. The Weck's reagent (1 g NaOH, 4 g KMnO₄, 100 ml H₂O) was used to etch the microsection [15]. The Vickers hardness was measured according to ISO 6507 by using the DuraScan 70 hardness tester at 5 N loading. The transverse samples of rectangular cross-section (GOST 1497–84, type 1, No. 22) (Fig. 2) were subjected to tensile test using the universal Super L 60 (Tinius Olsen) machine with the loading rate of 0.07 mm/sec. Local residual longitudinal deformations were estimated based on a change in distance between the tags pre-applied with the laser at 0.5 mm increments.

RESULTS AND DISCUSSION

Microstructure. The main difference between the two considered technologies is the mechanism of material joining during welding. In case of LW, a localized melting of metal occurs followed by the formation of a welded joint, which

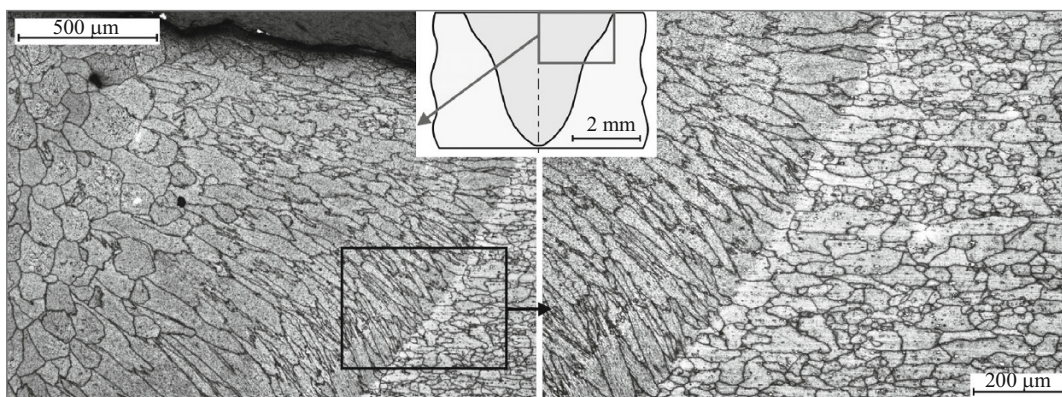


Fig. 3. Schematic of macrosection and microstructure of LW joint.

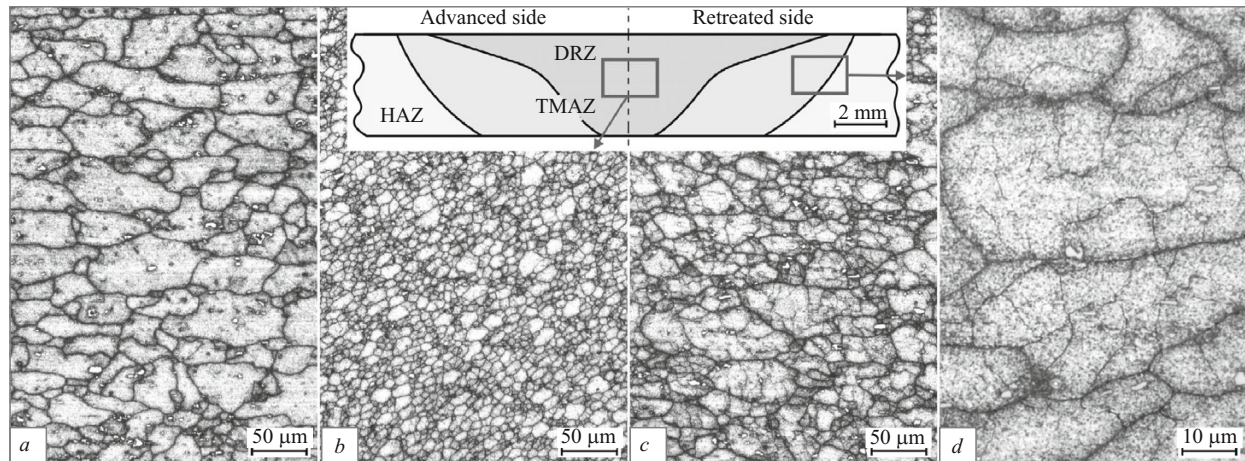


Fig. 4. Schematic of macrosection, microstructure of base metal 6082-T6 (a), dynamic recrystallization zones (b), and thermo-mechanically affected zones (c, d) of the FSW joint.

has a cast metal structure (Fig. 3). The cast metal structure of the LW joint contains dendrites growing from the joint border in the direction of the temperature gradient as the welding bath crystallizes, and equiaxed grains located along the longitudinal axis of the joint. The formation of these grains is caused by the fact that under high welding rates, a tear-drop-shaped bath of the molten metal is formed with the temperature gradient at the joint axis close to zero [17], which results in substantial concentration supercooling [18]. The equiaxed grains prevent dendrites from closing and forming an interlayer of liquid metal, which may lead to the formation of hot cracks along the joint axis under the effect of the pulling stresses during welding [19]. No visible changes in the microstructure of the HAZ were revealed by optical microscopy. The borders and extent of the HAZ could only be determined based on microhardness distribution.

In case of FSW, the metal is heated up due to heat generated by friction and intensive plastic deformation, but only to the level close to the solidus temperature [16], which results in the formation of a welded joint with the pronounced thermo-mechanically affected zone (TMAZ) (Fig. 4). When analyzing the FSW joints, the interface between HAZ and TMAZ is considered as a joint border. The microstructure of the thermo-mechanically affected zone is non-uniform. It includes an extensive area with the fine-grained structure (Fig. 4b), which is traditionally called a dynamic recrystallization zone (DRZ) [20]. The equiaxed DRZ grains have the size of 7.9 μm (No. 11 according to ASTM E112), which is 5.7 times less than the grains of the base metal (44.9 μm — No. 6) (Fig. 4a). Substantial plastic deformation of the metal during welding in combination with high heating temperatures facilitates the growth and dissolution of the dispersed β'' -phase particles, as well as redistribution and change in density of dislocations [21]. A thermo-mechanically affected zone comprising a mixture of grains, which have undergone polygonization and dynamic recrystallization, is readily visi-

ble between DRZ and HAZ (Fig. 4c and d). Grains with noticeable outlines of subgrain structure were also revealed (Fig. 4d).

Analysis of thermal cycles. It is known that mechanical properties of heat-treatable aluminum alloys are fully defined by the sizes, morphology and distribution of the precipitate particles [3, 4, 11, 21]. The processes of formation, growth and dissolution of the dispersed particles depend on the rate of thermal diffusion processes. The temperature field during welding determines the kinetics of the diffusion processes in a welded joint, and is described by two key parameters: maximum heating temperature of a specific point of the joint, and rates of heating/cooling or duration of exposure to specified temperatures.

The temperature field during welding depends on the spatial distribution of power of the heating source, as well as the welding rate. The analysis of experimentally measured thermal cycles in certain HAZ points (Fig. 5) showed that the heating time from the ambient to the maximum temperature during LW is 18 times longer compared to FSW, while the cooling time from the maximum temperature down to 100°C is half as long during LW. During FSW, the metal of the heat-affected zone is exposed to high temperatures for a longer period of time as compared to LW, specifically: 8 times longer at 200°C and above, and 11.5 times longer at 350°C and above (Fig. 5b). This facilitates the occurrence of the diffusion processes in the heat-affected zone, and as a result, causes a change in the mechanical properties.

During FSW, the maximum heating temperature of the plate surface at the tool shoulder reaches 509°C on the advanced side (Fig. 6b). At the same time, an asymmetry of the temperature field was revealed, which is caused by higher intensity of plastic deformation of metal on the advanced side, and as a result, enhanced generation of heat. This statement is in agreement with the experimental studies of the temperature field kinetics in the vicinity of the welding tool surface during welding [22].

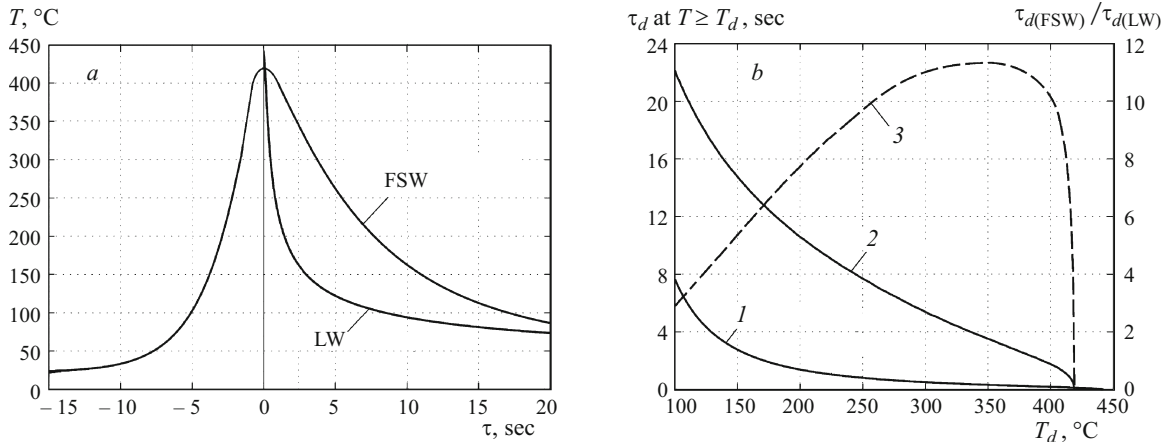


Fig. 5. Experimentally measured thermal cycles in the HAZ points on the plate surface during welding (*a*), and duration of metal exposure to a temperature in excess of the specified value (*b*): 1) LW-joint exposure time $\tau_{d(LW)}$; 2) FSW joint exposure time $\tau_{d(FSW)}$; 3) ratio $\tau_{d(FSW)}/\tau_{d(LW)}$.

The maximum temperature in the HAZ of the LW joint reaches the liquidus temperature (650°C) at the border of the joint (Fig. 6*a*). In combination with large temperature gradient in the cross-section of the joint and high heating/cooling rates, this leads to the formation of a narrow HAZ.

Microhardness of welded joints. A decrease in hardness in the HAZ of the LW joint is observed at a distance of less than 3.5 mm from the joint border and corresponds to heating above 260°C (Fig. 6*a*). A sharp decrease in hardness by 30% [from 112.5 HV (base metal) to 88 HV] occurs within 1.5 mm long section corresponding to the heating temperatures ranging from 260 to 320°C. This is caused by metal restructuring. Heating in excess of 320°C does not result in substantial changes in hardness due to an incomplete dissolution of the β'' -phase particles during welding and subsequent natural aging after cooling. This is supported by the fact that the hardness of this HAZ section exceeds that of the metal obtained after heat treatment according to T4 regimen. The minimum hardness of the welded joint constitutes 73.5 HV (65.3% of the hardness of the base metal) and corresponds to

the metal of the joint, which has undergone complete melting (Fig. 7*a*). Upon transition from the HAZ to the metal of the joint, a sharp decrease in hardness along the fusion line takes place — from 84 to 76 HV.

A decrease in hardness in the heat-affected zone of the FSW joint is observed within a 10 mm long section, which is 2.9 times more compared to LW (Fig. 6*b*). An asymmetry of the microhardness field was also revealed. More intensive generation of heat, and hence, lower hardness correspond to the advanced side of the welded joint. A decrease in hardness in the HAZ to 67 – 69 HV as the maximum heating temperature is increased to 350 °C represents a general tendency. A decrease in hardness below the level obtained after heat treatment of the base metal according to T4 regimen evidences the dissolution of the β'' -phase particles within this section of the HAZ with subsequent formation of the larger β' - and β -phase particles. This is in agreement with the data of the study [21], in which it was established that during the FSW thermal cycle, the solvus temperature of the β'' -phase particles corresponds to 353°C. At the distance of 1.65 –

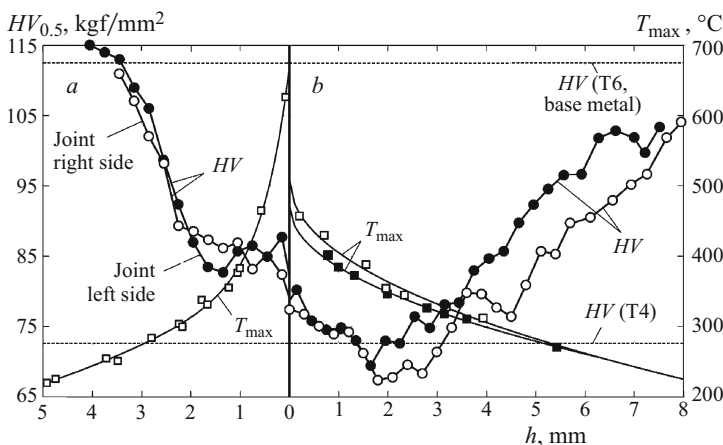


Fig. 6. Distribution of microhardness and maximum temperature in the HAZ of the welded joints produced by LW (*a*) and FSW (*b*): light symbols) advanced side; dark symbols) retreated side; *h*) distance from the joint border.

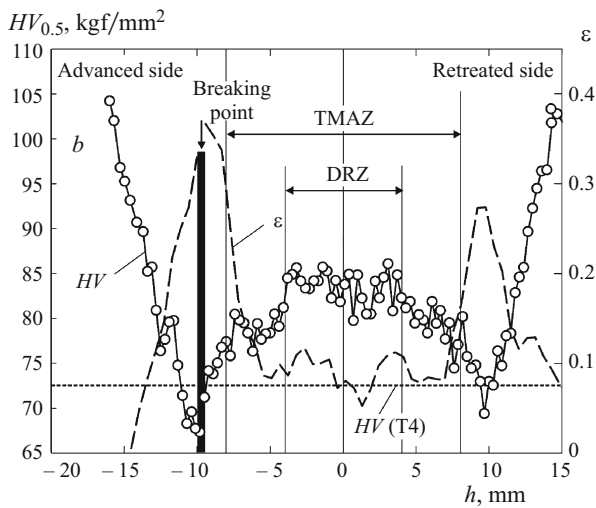
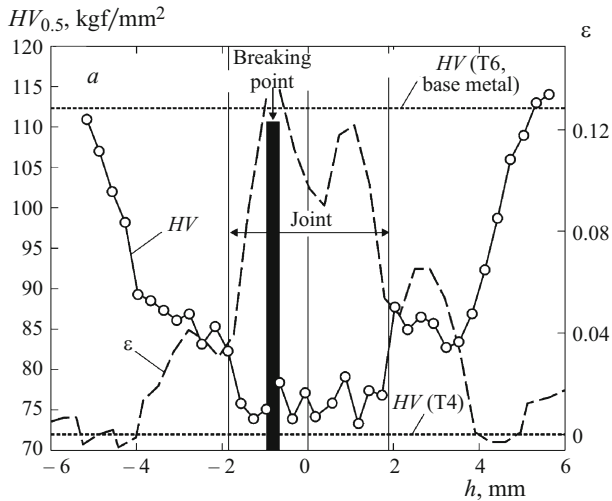


Fig. 7. Distribution of microhardness and residual plastic deformations in welded joints produced by LW (a) and FSW (b): h) distance from the center of the joint.

1.80 mm from the joint border, which corresponds to the heating range of 350 – 450°C, an increase in hardness is observed, which is caused by complete dissolution of the Mg_2Si phase particles. This process in combination with the natural aging after complete cooldown results in increases hardness. In the TMAZ of the joint, a gradual increase in hardness from 77 to 82 – 86 HV is observed upon transitioning from the joint border to the DRZ (Fig. 7b). Migration of dislocations during substantial plastic deformation of the metal in the DRZ and their interaction with dispersed particles in combination with high heating temperature facilitates an intensive dissolution of the dispersed particles. High density of dislocations in the deformed metal lowers the energy barrier for heterogeneous nucleation of the dispersed particles at these defects during natural aging. The minimum hardness of the welded joint constitutes 67.4 HV (60% of the hardness of the base metal) also corresponds to the HAZ of the advanced side.

TABLE 1. Mechanical Properties of Welded Joints

Treatment	σ_r , MPa	$\sigma_{0.2}$, MPa	δ , %
T6 regime (base metal)	340	298	22.0
Laser welding (joint)	227	213	1.7
Friction stir welding (joint)	245	181	4.2
T4 regimen (base metal)	260	149	28.0

The analysis of the hardness and temperature field distributions showed that at the same maximum heating temperature, the HAZ hardness during FSW is much lower compared to LW due to significantly lower rates of heating and cooling during FSW. Thus, at the same maximum temperature of 350°C, the hardness of the FSW joint is 20% lower than that of the LW-joint.

Mechanical properties. Non-uniformity of the welded joints with respect to the distribution and morphology of the dispersed Mg_2Si -phase particles determines the microhardness field and mechanical properties of the entire joint under tension. The tests have shown that both FSW and LW joints have approximately the same level of mechanical properties (see Table 1). The ratio between tensile strength of the welded joint and tensile strength of the base metal constitutes 0.72 for FSW and 0.67 for LW. The tensile strength of the FSW joints is close to that of the metal after heat treatment according to T4 regimen. The plasticity of the welded joints is lower than that of the base metal by 5.3 times in case of FSW and by 12.3 times in case of LW, which is caused by the concentration of deformations in the minimum hardness region (Fig. 7) and the presence of pores in the LW joints. It should be noted that the local plasticity of the HAZ is significantly higher than that of the joint (Fig. 7, Table 1). The concentration of the local plastic deformations occurs in the minimum hardness region, and the level of such deformation in the FSW joints is comparable to the metal heat-treated according to T4 regimen.

CONCLUSIONS

1. Welded joints produced by friction stir welding and laser welding using aluminum alloy 6082-T6 are characterized by distinct non-uniformity in microstructure and mechanical properties.

2. In the friction-stir welded joint, an asymmetry of the maximum temperature and microhardness fields was revealed.

3. The strength of the FSW joints constitutes 72%, and the strength of the LW joints constitutes 67% of the strength of the base metal. The plasticity of the welded joints is lower than that of the base metal by 5.3 times in case of the FSW, and by 12.3 times in case of the LW due to high concentration of deformations in the minimum hardness zone.

4. At the same maximum heating temperature, the HAZ hardness of the FSW joint was lower than that of the LW joint due to longer metal exposure to high temperatures.

5. The breaking point of the welded joints with transverse weld is determined by the minimum hardness zone.

This study was performed at the SPPU under the Contract No. 14.Z50.31.0018 with the Ministry of Education and Science of the Russian Federation.

REFERENCES

1. R. E. Trevisan, D. D. Schwemmer, and D. L. Olson, *The Fundamental of Weld Metal Pore Formation. Welding: Theory and Practice, Chap. 3*, Elsevier Science Pub. (1990).
2. R. J. Shore and R. B. McCauley, "Effect of porosity on high strength aluminum 7039," *Welding J.*, **49**(7), 311 – 321 (1970).
3. O. R. Myhr and O. Grong, "Process modelling applied to 6082-T6 aluminum weldments. I. Reaction kinetics," *Acta Mater.*, **39**, 2693 – 2702 (1991).
4. O. Grong, *Metallurgical Modelling of Welding*, The Institute of Materials, London (1997), 608 p.
5. J. Martikainen, E. Hiltunen, V. A. Karkhin, and S. Yu. Ivanov, "A method for evaluating the liquation cracking susceptibility of welded joints in Al – Mg – Si alloys," *Welding Int.*, No. 2, 139 – 143 (2013).
6. C. Huang and S. Kou, "Liquation cracking in full-penetration Al – Mg – Si welds," *Welding J.*, **83**(4), 111 – 122 (2004).
7. C. C. Chang, "Microstructure in hot cracking mechanism of welded aluminum alloys," *Mater. Sci. Technol.*, **29**(4), 504 – 510 (2013).
8. S. Katayama, *Handbook of Laser Welding Technologies*, Woodhead Publishing, 654 (2013).
9. U. Dilthey, A. Goumeniouk, V. Lopota, et al. "Development of a theory for alloying element losses during laser beam welding," *J. Phys. D: Appl. Phys.*, **34**(1), 81 – 86 (2001).
10. S. W. Kallee, "Industrial applications in friction stir welding," in: D. Lohwasser and Z. Chen (eds). *Friction Stir Welding. From Basic to Applications*, Woodhead Publishing, Cambridge (2010), pp. 118 – 163.
11. C. Gallais, A. Simar, D. Fabregue, et al. "Multiscale analysis of the strength and ductility of AA6056 aluminum friction stir welds," *Metall. Mater. Trans.*, **38A**, 964 – 981 (2007).
12. C. A. Weis Olea, "Influence of energy input in friction stir welding on structure evolution and mechanical behaviour of precipitation-hardening in aluminium alloys (AA2024-T351, AA6013-T6 and Al – Mg – Sc)," GKSS-Forschungszentrum Geesthacht GmbH, 149 (2008).
13. T. Morita and M. Yamanaka, "Microstructural evolution and mechanical properties of friction-stir-welded Al – Mg – Si joint," *Mater. Sci. Eng. A*, **595**(10), 196 – 204 (2014).
14. O. V. Velichko, S. Yu. Ivanov, V. A. Karkhin, et al. "Friction stir welding of thick plates of Al – Mg – Sc alloy," *Welding Int.*, **30**(8), 630 – 634 (2016).
15. *ASM Handbook, Vol. 9: Metallography and Microstructures ASM International*, Materials Park, Ohio, USA (2004), 1184 p.
16. P. Upadhyay and A. Reynolds, "Effect of backing plate thermal property on friction stir welding of 25-mm-thick AA6061," *Metall. Mater. Trans. A*, **45**, 2091 – 2100 (2014).
17. V. A. Karkhin, A. S. Ilin, H. J. Pesch, et al. "Effects of latent heat of fusion on thermal processes in laser welding of aluminum alloys," *Sci. Technol. Welding Joining*, **10**(5), 597 – 603 (2005).
18. P. Rayamyaki, V. A. Karkhin, P. N. Khomich, "Determination of the main characteristics of the temperature field for the evaluation of the type of solidification of weld metal in fusion welding," *Welding Int.*, **21**(7), 600 – 604 (2007).
19. V. Ploshikhin, A. Prikhodovskii, M. Makhutin, et al. "Integrated mechanical-metallurgical approach to modeling of solidification cracking in welds," in: T. Boellinghaus and H. Herold (eds.), *Hot Cracking Phenomena in Welds*, Springer (2005), pp. 223 – 244.
20. P. L. Threadgill, A. J. Leonard, H. R. Shercliff, and P. J. Withers, "Friction stir welding of aluminum alloys," *Int. Mater. Rev.*, **54**(2), 49 – 93 (2009).
21. Y. S. Sato, H. Kokawa, M. Enomoto, and S. Jogan, "Microstructural evolution of 6063 aluminum during friction-stir welding," *Metall. Mater. Trans. A*, **30**(9), 2429 – 2437 (1999).
22. A. Fehrenbacher, N. A. Duffie, N. J. Ferrier, et al. "Temperature measurement and closed-loop control in friction stir welding," in: *8th International Friction Stir Welding Symposium*, Timmendorfer Strand, Germany (2010), 19 p.